



Analysis of the upscaling problem – A case study for the barotropic dynamics in the North Sea and the German Bight



J. Schulz-Stellenfleth*, E.V. Stanev

Helmholtz-Zentrum Geesthacht (HZG), Max-Planck-Str. 1, 21502 Geesthacht, Germany

ARTICLE INFO

Article history:

Received 1 September 2015

Revised 30 November 2015

Accepted 6 February 2016

Available online 23 February 2016

Keywords:

Upscaling
Ocean model
Tides

ABSTRACT

The upscaling problem is investigated using the barotropic dynamics of the North Sea and the German Bight as an example. The impact of small scale perturbations of bathymetry, bottom roughness, wind forcing, and boundary forcing is quantified using a two-dimensional linear barotropic model for the entire North Sea with 5 km resolution. The model is solved in the spectral domain for the dominant M2 tide. Comparisons with results from a fully nonlinear 3D circulation model show that the main circulation features are well captured by the spectral model. The impact of different types of perturbations is estimated by inversion of the model using the perturbation covariance matrix as input. Case studies with white noise and fully correlated noise are presented. It is shown that the German Bight area stands out in its sensitivity with respect to small scale uncertainties of bathymetry. Small scale changes of bottom roughness have a particularly strong effect in the English Channel. Small scale wind perturbations have a significant local effect only in very shallow near coastal areas. It is shown that uncorrelated noise introduced along an open boundary around the German Bight only has a very local effect. Perturbations with long correlation length are shown to lead to significant far field effects along the east coast of England. It is demonstrated that this effect is related to the boundary conditions used for the North Sea model. In a next step a German Bight grid with 1 km resolution is nested into the North Sea grid and the spectral model is solved in a two way nested configuration. It is shown that there are some significant local and far field effects caused by the change of resolution in this coastal area. Finally, the potential impact of observations taken in coastal areas is investigated by evaluating the Kalman a posteriori distribution of analysis vectors based on different assumptions about model errors. The area of influence of a single tide gauge is quantified for the case where the model errors are dominated by boundary forcing errors. The results show a strong dependence on spatial correlation properties of the errors.

© 2016 Elsevier Ltd. All rights reserved.

1. Introduction

There is an increasing number of coastal observatories becoming operational worldwide (Kourafalou et al., 2015; Stanev et al., 2011; Riethmüller et al., 2009; Howarth and Palmer, 2011; Bolaños et al., 2009). This development is in particular driven by the growing need for information on coastal processes relevant for the planning and management of human activities like, e.g., offshore wind farming. At the same time, big efforts are made in different parts of the world to setup operational models for the regional scale. For example, in Europe these activities are now organised in the framework of the COPERNICUS program (<http://www.copernicus.eu/>), which ensures that consistent regional model forecasts are provided for all European coastal areas.

Regional models, like the North West Shelf model used in COPERNICUS, are not able to resolve all relevant coastal processes. Downstream services for user groups interested in coastal information usually require higher spatial resolution. The usual approach to solve this problem is a nested setup, where a high resolution coastal model is coupled to a coarser model (also called “parent model”) using either one-way or two-way coupling methods (Barth et al., 2005). Alternatively, unstructured grid models are used to realize a seamless transition between different spatial scales (Zhang et al., 2015). Due to the high computational costs, the use of these models for operational applications is still limited up to now.

Also, the assimilation of observation data usually requires the use of high resolution models, because a lot of the small scale processes, e.g., monitored by HF radar systems (Paduan and Washburn, 2012; Stanev et al., 2015), cannot be reproduced by regional scale models. To make best use of coastal observations and to improve both coastal and regional scale forecasts different aspects of nested model coupling require detailed analysis.

* Corresponding author. Tel.: +49 415287 1511.

E-mail address: johannes.schulz-stellenfleth@hzg.de (J. Schulz-Stellenfleth).

Nomenclature

a_u, a_v	amplitudes of zonal and meridional current components [m s ⁻¹]
A	Jacobian matrix of the linear spectral tide model
\mathbf{b}	right hand side of linear model equation
E	energy density [kg s ⁻²]
ϵ	observation error vector
ϵ_{diss}	energy dissipation [kg s ⁻³]
f	Coriolis parameter [s ⁻¹]
φ_u, φ_v	phases of zonal and meridional current components [rad]
Φ_x, Φ_y	energy fluxes in zonal and meridional direction [kg m s ⁻³]
g	gravitational acceleration [m s ⁻²]
G	observation error covariance matrix
h	water depth [m]
H	observation operator matrix
K	Kalman gain matrix
i	imaginary unit
I_n	identity matrix of dimension n
ω	angular frequency [rad s ⁻¹]
λ_w	wind drag coefficient
n	model state vector dimension
n_{ob}	number of points along German Bight open boundary
n_{int}	number of interior grid points
O_n	matrix of dimension $n \times n$ filled with ones
P	model error covariance matrix
Q	covariance matrix of perturbation vector
r	bottom friction coefficient
r_1	scaled bottom friction coefficient [m s ⁻¹]
ρ	density of sea water [kg m ⁻³]
σ_h	standard deviation of bathymetry perturbation [m]
σ_{ob}	standard deviation of open boundary forcing perturbation
σ_r	standard deviation of bottom roughness perturbation [m s ⁻¹]
t	time [s]
$\tau_{bott}^x, \tau_{bott}^y$	bottom friction terms for zonal and meridional component [m ² s ⁻²]
U, V	zonal and meridional transport components [m ² /s]
\hat{u}, \hat{v}	complex Fourier coefficient for zonal and meridional transport [m ² /s]
$\hat{U}_{10}, \hat{V}_{10}$	complex Fourier coefficients for zonal and meridional 10 m wind [m/s]
x, y	zonal and meridional coordinates [m]
\mathbf{x}	model state vector
\mathbf{y}_{obs}	observation vector
ζ	water elevation [m]
$\hat{\zeta}$	complex Fourier coefficient for water elevation [m]

The problem becomes evident looking at the case of the North Sea and the German Bight as an example. For the entire North Sea operational regional model forecasts with about 5 km spatial resolution are available either from the COPERNICUS system or the system run at the Federal Maritime and Hydrographic Agency (BSH) (Dick et al., 2001). At the same time, a large variety of observations is available in the German Bight provided by the Coastal Observing System for Northern and Arctic Seas (COSYNA) (Stanev et al., 2011). The system includes observations with large coverage and

high spatial resolution, like HF radar (Stanev et al., 2015), as well as detailed observations of the vertical structure, e.g., by gliders (Merckelbach, 2013).

At the very beginning of the present study we want to address the used terminology. In flow physics the distribution of energy over different spatial and temporal scales is not only determined by the forcing, but also to a large extent by the re-distribution of energy due to non-linear interaction processes (Nastrom et al., 1984). One important question is whether intermediate scales (in our case regional scales) obtain their energy from a large-scale motion (e.g., Kelvin wave) or from small-scales (e.g., coastal processes, which are largely turbulent). It is usually accepted that larger scale eddies disintegrate into smaller ones, dissipating their energy into smaller length scales. At the smallest length scales, the viscosity becomes important and the energy dissipates into heat. In the theory of 2D turbulence (Kraichnan, 1967) an inverse energy cascade is supported (from small to large scales). While 2D flows do not transfer energy downscale, the 3D turbulence does not support an upscale energy transfer. In the above description of the basic flow dynamics up-and-down-scale transfer is understood as transfer of energy to larger or smaller scales. This sometimes leads to a spectral condensation and enhancement of motion at specific scales coherent over the entire domain or part of it (Sommeria, 1986). It is also known that systems with long memory (the ocean) integrate stochastic forcing, thereby transforming a white-noise signal into a red-noise one (Hasselmann, 1976).

In meteorology and oceanography under downscaling, one understands a procedure to take information known at large scales to make predictions at local scales. Dynamical downscaling implies using a high-resolution model in a sub-domain forced at its boundaries by output from a lower-resolution model. Statistical downscaling necessitates the development of statistical relationships between local variables (e.g., SST) and large-scale predictors (e.g., atmospheric pressure). In a second step these relationships are applied to the output of large-scale models to reconstruct local variables. Both approaches result in fine resolution predictions in limited areas. Obviously, it is not straightforward to define upscaling in atmospheric and ocean science as exactly the opposite to downscaling. Therefore, we will be following the ideas developed in fluid dynamics and will consider upscaling as a process in which information is transferred from a smaller scale to a larger scale. If this concept is applied to the spatial dimension, one can define a separation length scale s_{sep} and study the impact of processes with correlation length less than s_{sep} on processes with correlation length larger than s_{sep} . This aspect will be treated in this study to some extent, but the definition for upscaling used here is a little bit wider and more tailored to the problem of matching the coastal and regional scale in ocean modelling. In particular, we will study the large scale impact of signals originating either from boundary forcing along a coastal domain or from near shore measurements. We will also investigate the impact of perturbations introduced into the model at the smallest resolved scale, i.e., white noise. These different aspects of the upscaling problem are analysed using the tidal dynamics in the North Sea and the German Bight as an example. We have concentrated on the barotropic part because this allows a quite rigorous statistical treatment of the problem.

The North Sea is a shallow shelf sea with mean water depth of 80 m and a maximum depth of about 800 m (in the Norwegian Trench). An overview map of the north west shelf area with the North Sea and its surrounding seas is shown in Fig. 1a. The dashed line indicates the 200 m isobath.

The tides in the North Sea are triggered by the Atlantic semi-diurnal Kelvin wave, which travels from south to north along the continental shelf. Energy is transmitted across the shelf edge into the Celtic Sea between Brittany and southern Ireland. This wave

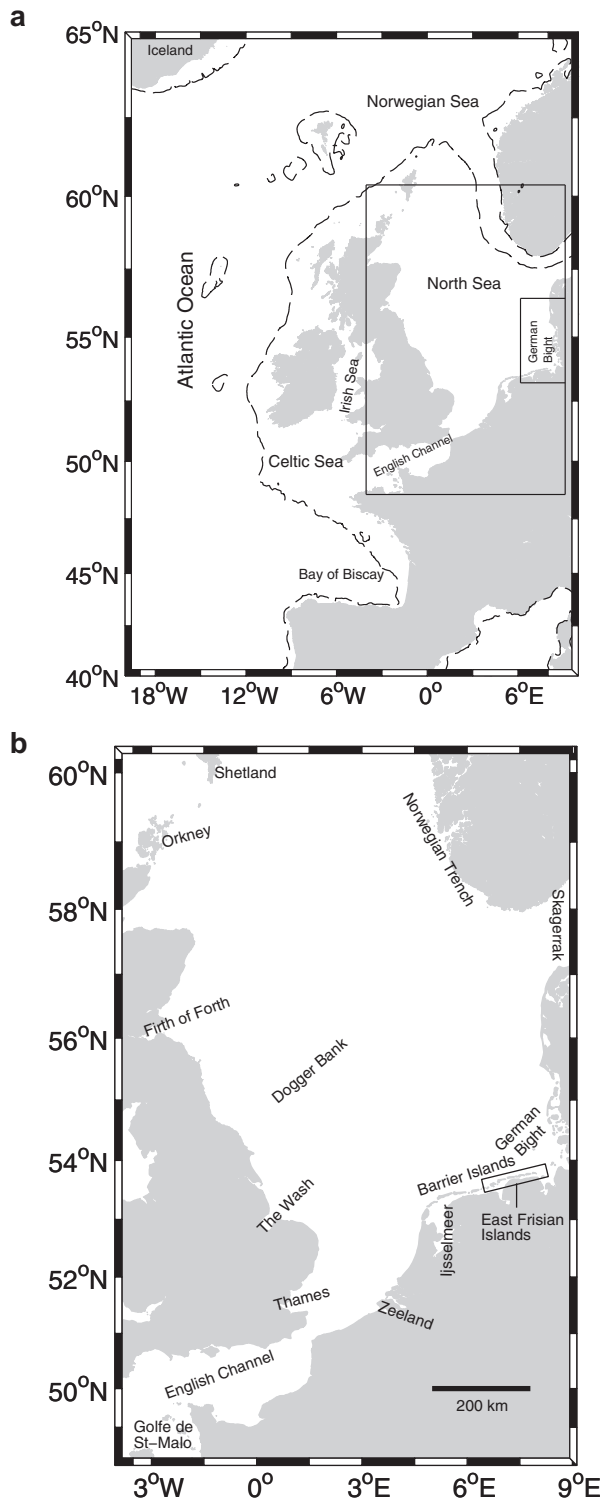


Fig. 1. (a) Map of the European North West Shelf area. The dashed line is the 200 m isobath. The two rectangles indicate numerical model domains used in the study. (b) Zoom into North Sea with some geographical locations mentioned in the text.

then propagates into the English Channel where some of the energy is passed on into the southern North Sea through the Dover strait. The Atlantic wave progresses northwards, taking five hours to travel from the Celtic Sea along the continental shelf to the Shetlands where it feeds more energy into the tidal dynamics of the North Sea (e.g., Pugh, 1996). A more detailed map of the North Sea with some geographical locations mentioned in

the text is shown in Fig. 1b. Overviews of the full three dimensional North Sea dynamics and more information on tides can be found in Sündermann and Pohlmann (2011), Otto et al. (1990), and Andersen et al. (2006).

Perturbations on the coastal scale can be introduced by either observations, which are used in an assimilation system to modify the state inside the coastal model, or by modifications of parameters in the coastal model. In both cases an important question is how the radius of impact depends on the type of perturbation and the setup of the nested system. In this study we will concentrate on the following questions:

- What is the effect of small scale perturbations of model variables (e.g., bathymetry or bottom roughness) on the regional scale?
- What is the effect of perturbations applied in coastal areas on the regional scale?
- How do these effects depend on correlation properties of the perturbation?
- How do these effects depend on the boundary conditions used for the regional model?

To keep the analysis simple and to allow a rigorous statistical treatment, the study employs a linear two dimensional (2D) barotropic model. The main advantage of this approach is that sensitivity experiments can be performed without the need of Monte Carlo runs like, e.g., used in Mourre et al. (2004). Statistical parameters can be computed directly from the governing Navier Stokes equations making appropriate assumptions about variance and correlation properties of the perturbations. Data from a nonlinear 3D circulation model were used to provide realistic boundary forcing.

It should be noted that other tools exist to perform sensitivity studies like presented here. For example, the Regional Ocean Modeling System (ROMS) (Shchepetkin and McWilliams, 2005), which resolves the full nonlinear three-dimensional barotropic and baroclinic dynamics, comprises inverse models (Di Lorenzo et al., 2007; Moore et al., 2004), which have been successfully used for sensitivity assessments and data assimilation in previous studies (Moore et al., 2009; Veneziani et al., 2009).

There are a couple of reasons, why we decided to use a simpler linear model approach in our analysis. First of all, we are dealing with small perturbations in this study, for which linear approximations usually work quite well. This is nicely demonstrated by the successful use of adjoint models, which represent linear approximations as well. Secondly, the model used here allows a clear separation of the impact on the tidal dynamics without the need to consider issues like model spinup or spectral estimation errors associated with finite model run periods. Furthermore, the model is simple enough to allow a complete description of the underlying equations and parameters in the text. The basis for the study is therefore very clear and allows a re-production of results by readers. Finally, the used model is computationally efficient and very flexible. This became particularly evident, when we were able to use the approach to solve a nested two-way coupled problem in a very straightforward way.

The paper is structured as follows. In Section 2 the linear model used for the analysis is introduced. In Section 3 some general results about the density, the flux, and the dissipation of energy are presented. Section 4 is about the general approach of the sensitivity analysis using the inverse model. In Section 5 this method is applied to study the large scale impact of white noise perturbations introduced into the model. This is followed by an analysis of the effect of boundary forcing perturbations added along the German Bight boundary in Section 6. In Section 7 a coarse resolution North Sea model is two-way coupled to a high resolution German Bight model using the linear model. Results with and without nesting are compared. Section 8 is about the large scale impact

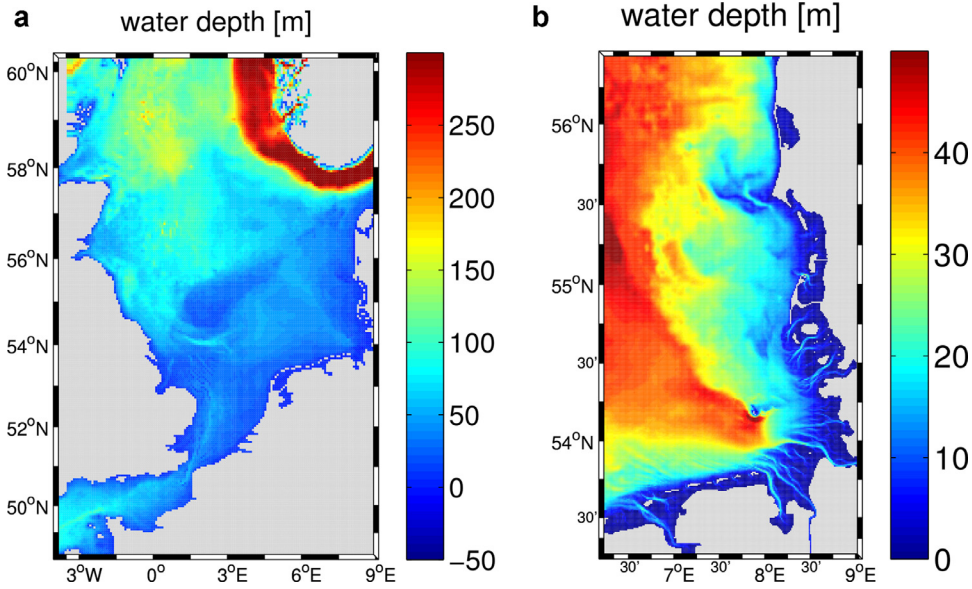


Fig. 2. Bathymetry for the North Sea with 5 km resolution (a) and the German Bight with 1 km resolution (b).

of observations taken in a coastal area followed by conclusions in Section 9.

2. Numerical models used

In this section the numerical models and model data used in this study are introduced. We will start with the linear model, which is used as a basis for the statistical analysis. The most important approximations are mentioned and the numerical method to solve the equations is explained. This model was run on a grid covering the entire North Sea and a second grid with higher resolution covering only the German Bight as depicted by the two rectangles in Fig. 1a. Note that the latter grid actually covers a bit more than the geographical area of the German Bight, but this is the domain used in the BSH coastal model (Dick et al., 2001), and we will refer to it as the German Bight grid for simplicity. The respective bathymetries are shown in Fig. 2. The North Sea grid has 5 km resolution and the German Bight grid has 1 km resolution. The grid dimensions are 159×237 for the coarse grid and 210×287 for the fine grid. Both grids are also used in the operational BSH system (Dick et al., 2001).

The linearised Navier Stokes equations in two dimensions read (e.g., Maier-Reimer, 1977)

$$\frac{\partial \zeta}{\partial t} + \frac{\partial U}{\partial x} + \frac{\partial V}{\partial y} = 0 \quad (1)$$

$$\frac{\partial U}{\partial t} - fV + gh \frac{\partial \zeta}{\partial x} + \tau_{bott}^x = \lambda_W \sqrt{U_{10}^2 + V_{10}^2} U_{10} \quad (2)$$

$$\frac{\partial V}{\partial t} + fU + gh \frac{\partial \zeta}{\partial y} + \tau_{bott}^y = \lambda_W \sqrt{U_{10}^2 + V_{10}^2} V_{10}, \quad (3)$$

where g denotes gravitational acceleration, f is the Coriolis parameter, h is water depth, and ζ is water elevation. U and V denote the transport, i.e., $U = hu$ and $V = hv$, where u and v are the vertical mean current speeds in zonal and meridional direction. U_{10} and V_{10} are the zonal and meridional wind speed components at 10 m height and λ_W is the wind drag coefficient. For the most part of the study we will concentrate on the pure tidal dynamics and analyse the momentum equations with $\lambda_W = 0$. For the studies including wind forcing we have used $\lambda_W = 3.2 \cdot 10^{-6}$ following Backhaus (1976). For the bottom friction terms τ_{bott}^x , τ_{bott}^y the stan-

dard quadratic expression is given as (Maier-Reimer, 1977; Backhaus, 1976)

$$\tau_{bott}^x = r \sqrt{u^2 + v^2} u \quad (4)$$

$$\tau_{bott}^y = r \sqrt{u^2 + v^2} v \quad (5)$$

with vertical mean current speeds in zonal and meridional direction u, v and bottom friction coefficient r . To linearise these expressions an average of the square root factor was estimated by assuming that the dynamics is dominated by one tidal constituent. For the North Sea, which is dominated by the semidiurnal M2 tide, this is a reasonable assumption. If the respective amplitudes for u and v are given by a_u and a_v , we have

$$\begin{aligned} \langle u^2 + v^2 \rangle &= \frac{1}{2\pi} \int_0^{2\pi} a_u^2 \cos^2(\varphi - \varphi_u) + a_v^2 \cos^2(\varphi - \varphi_v) d\varphi \\ &= \frac{1}{2} (a_u^2 + a_v^2), \end{aligned} \quad (6)$$

where φ_u and φ_v are the respective phase offsets. If the square root in Eqs. (4), and (5) is linearised around this mean values and once again averaged over one tidal cycle, one gets

$$\langle \sqrt{u^2 + v^2} \rangle \approx \sqrt{\frac{1}{2} (a_u^2 + a_v^2)}, \quad (7)$$

and the bottom stress terms can thus be approximated as

$$\tau_{bott}^x \approx \frac{r}{h} \sqrt{\frac{1}{2} (a_u^2 + a_v^2)} U \quad (8)$$

$$\tau_{bott}^y \approx \frac{r}{h} \sqrt{\frac{1}{2} (a_u^2 + a_v^2)} V. \quad (9)$$

Values for the amplitudes a_u and a_v can be obtained either from a reference run or using an iteration scheme as explained later on. A value of $r = 0.0025$ as in Maier-Reimer (1977) was used for the friction coefficient. For brevity we will use the definition

$$r_1 = r \sqrt{\frac{1}{2} (a_u^2 + a_v^2)} \quad (10)$$

in the following.

As a next step, a complex periodic ansatz for the three prognostic variables is used (Provost et al., 1981; Barth et al., 2009), i.e.,

$$\begin{aligned}\zeta(x, y, t) &= \hat{\zeta}(x, y) e^{-i\omega t} \\ U(x, y, t) &= \hat{u}(x, y) e^{-i\omega t} \\ V(x, y, t) &= \hat{v}(x, y) e^{-i\omega t}.\end{aligned}\quad (11)$$

Here, ω is a given angular tidal frequency, t is time, i is the imaginary unit, $\hat{\zeta}$, \hat{u} , \hat{v} are the complex Fourier coefficients for elevation and the two velocity components, and x , y denote the zonal and meridional coordinates. Using these definitions, the continuity and momentum equations can be rewritten as

$$-i\omega \hat{\zeta} + \frac{\partial \hat{u}}{\partial x} + \frac{\partial \hat{v}}{\partial y} = 0 \quad (12)$$

$$-i\omega \hat{u} - f \hat{v} + gh \frac{\partial \hat{\zeta}}{\partial x} + \frac{r_1}{h} \hat{u} = \lambda_w \hat{U}_{10} \quad (13)$$

$$-i\omega \hat{v} + f \hat{u} + gh \frac{\partial \hat{\zeta}}{\partial y} + \frac{r_1}{h} \hat{v} = \lambda_w \hat{V}_{10}, \quad (14)$$

where \hat{U}_{10} and \hat{V}_{10} are the complex Fourier coefficients associated with the ω frequency component of the wind forcing terms in Eqs. (2) and (3).

It is important to emphasize that these equations refer to the tidal dynamics only. In reality, additional driving mechanisms exist, which are associated with ocean waves, or density gradients. Due to nonlinear terms in the dynamical equations (e.g., bottom friction) complex interactions occur (Hashemi et al., 2014). However, in this study the focus is on a first order sensitivity analysis, in which higher order coupling processes can be neglected. The integration of additional physical processes into the analysis will be the subject of future studies.

The system of Eqs. (12)–(14) was discretized on a standard Arakawa C-grid resulting in the following complex banded linear system of dimension $n = 3n_w$

$$\mathbf{Ax} = \mathbf{b}, \quad (15)$$

where n_w is the number of wet points. Here, A is a banded complex matrix of dimension $n \times n$, and \mathbf{b} is a complex vector of dimension n , which contains the open boundary forcing, the meteorological forcing, and zeros. The vector \mathbf{x} represents the model state and contains the complex amplitudes of the two velocity components \hat{u} , \hat{v} and the elevation $\hat{\zeta}$. The linear system was solved using the routine ZGBSV provided by the FORTRAN LAPACK library. For the North Sea domain one gets $n = 113,049$ and for the German Bight domain we have $n = 243,810$.

The system was first solved for the M2 tidal component with angular frequency

$$\omega_{M2} = \frac{2\pi}{12.42 \text{ h}}. \quad (16)$$

The North Sea bathymetry shown in Fig. 2a was used for the first experiments. Clamped boundary conditions were imposed for the open boundaries in the English Channel, the Skagerrak and along the boundary to the Norwegian Sea.

The required M2 amplitudes and phases were estimated from output of the operational BSH model (Dick et al., 2001). This circulation model is three-dimensional and takes into account meteorological forecasts for the North Sea and Baltic Sea provided by the German Weather Service (DWD), tides and external surges entering the North Sea from the Atlantic, as well as river runoff from the major rivers. One year of half-hourly output of waterlevels was used to estimate complex M2 tidal coefficients at the open boundaries.

To deal with the bottom friction term in the momentum Eqs. (13), and (14) a simple fixed-point iteration scheme was applied. The linear system was first solved using a first guess for a_u and a_v ($a_u = a_v = 1 \text{ ms}^{-1}$). Then the resulting amplitudes for u and v were used to solve the system again. This procedure was repeated until convergence occurred. Typically, the velocity field updates dropped below 1 mm/s within 30 iterations. It has to be pointed out that this method does not provide a complete treatment of nonlinear bottom friction processes. In particular, this approach is not able to generate higher harmonics, seen in fully nonlinear models, because the phase information in the nonlinear term is dropped.

Fig. 3 shows a comparison of the phase and amplitudes computed with the linear model with the respective values estimated from the operational BSH model. As one can see, the main features like, e.g., the position of the two amphidromic points and the distribution of energy, are well captured by the linear model. There are some differences in the amplitudes visible, in particular along the English coast and in the German Bight, but overall these results show that the linear model is well suited for sensitivity studies, which concentrate on first order mechanisms.

3. Density, fluxes and dissipation of energy

In this section a short overview of some of the general features of the tidal North Sea dynamics in terms of energy fluxes and dissipation is given. It has to be emphasized that the flux and dissipation values obtained with the linear model have to be regarded as rough estimates. The objective here is to give a qualitative picture of the general dynamics.

The energy density per unit area, averaged over one tidal cycle, is given by

$$E = 0.25 \rho \left(g |\hat{\zeta}|^2 + \frac{1}{h} (|\hat{u}|^2 + |\hat{v}|^2) \right), \quad (17)$$

with sea water density ρ . This expression contains both the potential energy associated with surface elevations and kinetic energy due to currents. Fig. 4a shows a map of energy density estimated from the linear model. One can see that the highest values are observed along the English east coast and the English Channel. Although the energy is significantly smaller in the German Bight, it still exceeds the low values observed in the central and north eastern North Sea.

The bottom stress vector is given as (Munk, 1997)

$$\bar{\tau}_{\text{bott}} = -r_1 \rho \begin{pmatrix} u \\ v \end{pmatrix}, \quad (18)$$

where we have used the definition in Eq. (10). The dissipation then follows as

$$\epsilon_{\text{diss}} = r_1 \rho (u^2 + v^2). \quad (19)$$

For the dissipation, averaged over one tidal cycle, we thus get

$$\langle \epsilon_{\text{diss}} \rangle = 2^{-3/2} r \rho (a_u^2 + a_v^2)^{3/2} \quad (20)$$

with tidal amplitudes for the zonal and meridional current component a_u , a_v . Fig. 4b shows respective dissipation values estimated from the linear model. In this case we see the strongest values in the English Channel and along the south east part of the English coast. The velocity amplitudes for the meridional and zonal currents shown in Fig. 5 indicate that this strong dissipation is associated with large current magnitudes in those areas. The German Bight shows the highest dissipation values in the eastern part of the North Sea. Again, it can be seen that this is related to relatively large values for the zonal current component.

The energy fluxes per unit length in zonal and meridional direction, averaged over one tidal cycle, are given by (Pugh, 1996)

$$\Phi_x = 0.5 \rho g h |\hat{\zeta}| |\hat{u}| \cos(\arg(\hat{\zeta}) - \arg(\hat{u})), \quad (21)$$

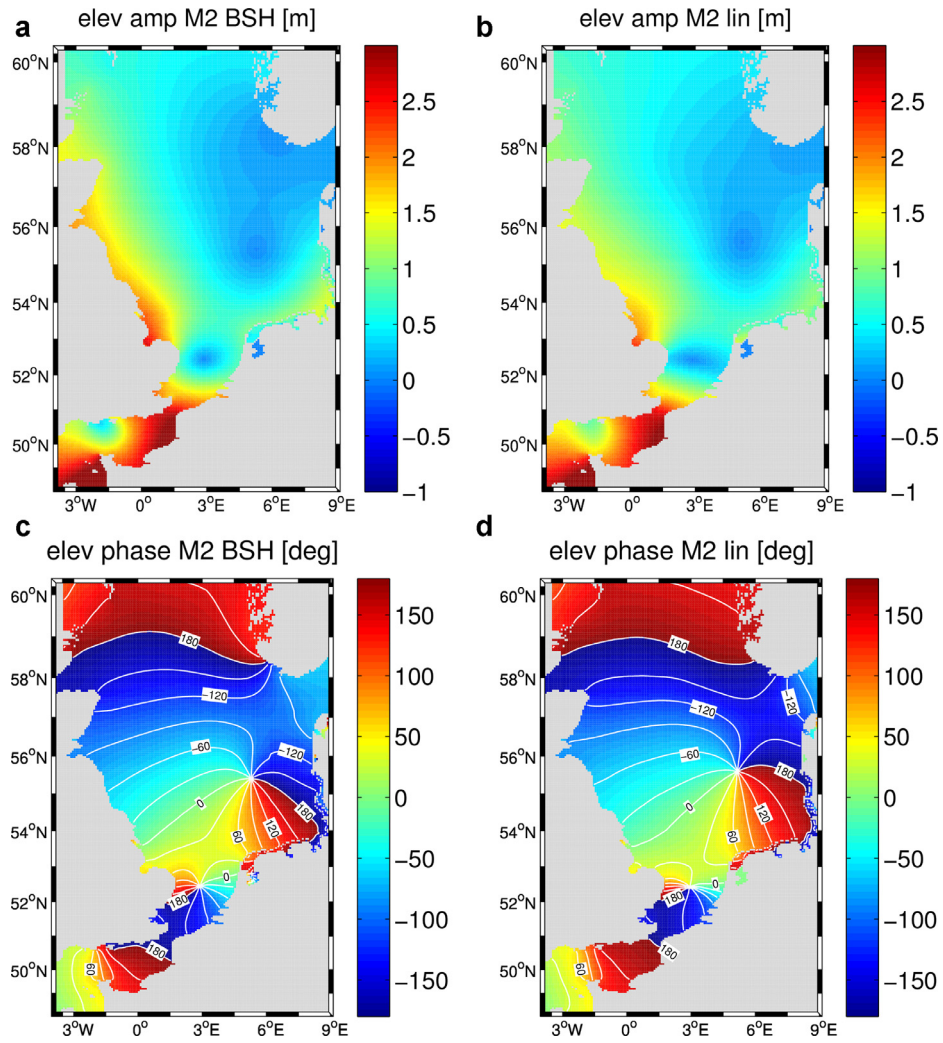


Fig. 3. Comparison of M2 amplitudes (a, b) and phases (c, d) for the operational BSH model (a, c) and the linear spectral model (b, d).

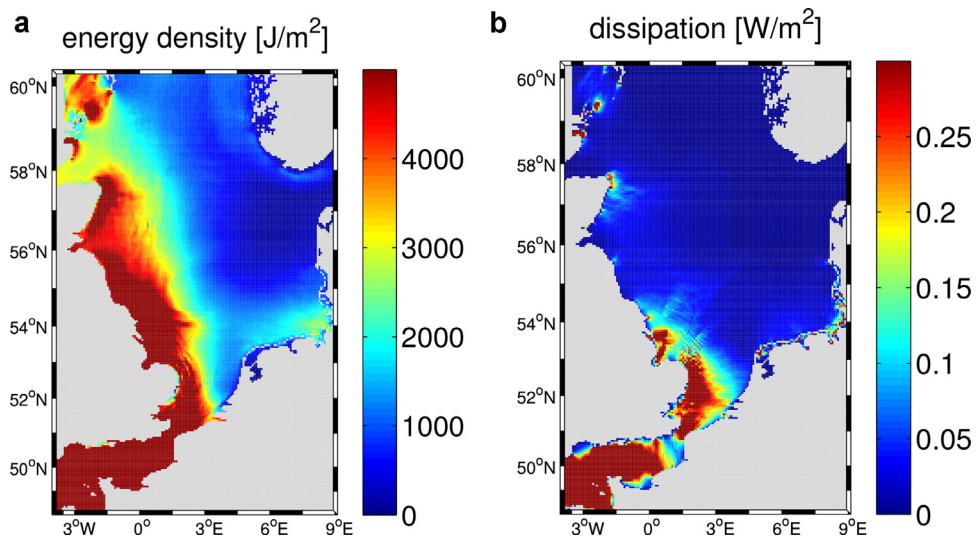


Fig. 4. M2 energy density (a) and energy dissipation (b).

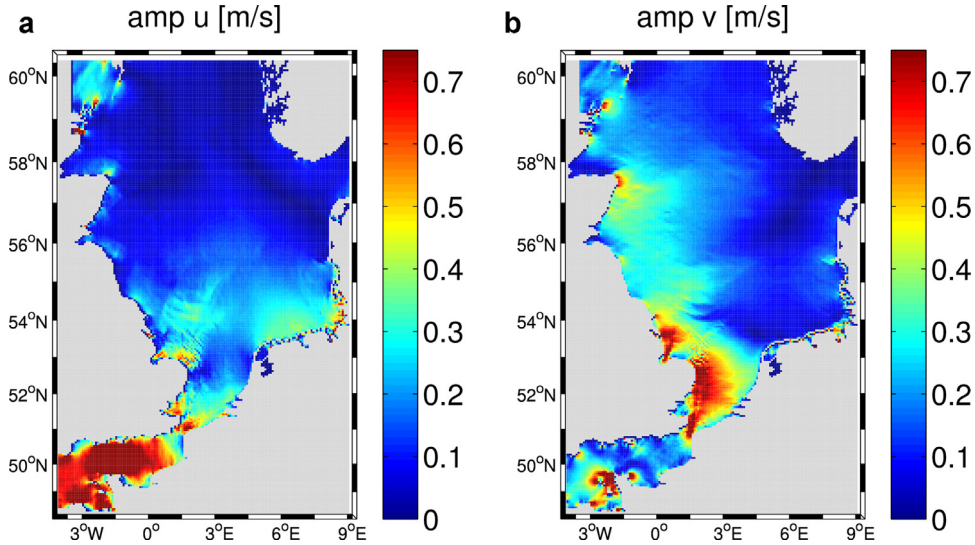


Fig. 5. M2 amplitude of zonal (a) and meridional (b) current speeds.

$$\Phi_y = 0.5 \rho g h |\hat{\zeta}| |\hat{v}| \cos(\arg(\hat{\zeta}) - \arg(\hat{v})), \quad (22)$$

where \arg denotes the argument of a complex number. The energy flux can thus be readily estimated from the linear model introduced in the previous section. Fig. 6 shows respective vector maps for the entire North Sea (Fig. 6a) and a zoom into the German Bight (Fig. 6b) with different scaling of the arrow lengths. One can see that the strongest energy fluxes can be found along the English east coast and in the English Channel. Both branches of energy fluxes transport energy into the area of high dissipation seen in Fig. 4b. The fluxes inside the German Bight are about one order of magnitude smaller with the strongest flux values found in the southern part along the East Frisian Islands. These findings are well consistent with previous studies, which were based on three-dimensional nonlinear models (e.g., Davies and Kwong, 2000).

4. Statistical analysis using the inverse model

In this section the basic statistical analysis method is explained, which is employed in the following sensitivity studies. Applying parallelisation techniques and using a cluster computer it is feasible to invert the matrix A in the linear system given by Eq. (15). We can then write

$$\mathbf{x} = A^{-1} \mathbf{b}, \quad (23)$$

which allows us to analyse the sensitivity of the barotropic North Sea dynamics with respect to the open boundary forcing also in statistical terms. In the following we assume that the boundary forcing is a zero mean complex Gaussian process with prescribed variances $\sigma_k^2 = \langle |b_k|^2 \rangle$. The resulting covariance matrix of the state vector is then given by

$$\langle \mathbf{x} \mathbf{x}^H \rangle = A^{-1} \langle \mathbf{b} \mathbf{b}^H \rangle (A^{-1})^H, \quad (24)$$

with superscript H denoting conjugate transpose. If we want to compute the variance of a specific component of the state vector, we thus need the respective line of the matrix A^{-1} . In order to avoid storage of the entire inverse matrix, which does not have a banded structure like the original matrix A , one can use the identity

$$(A^{-1})^T = (A^T)^{-1}, \quad (25)$$

i.e., the rows of A^{-1} can be obtained as columns of the inverse of A^T . These columns can be easily computed step by step solving the

linear systems defined as

$$A^T \mathbf{c}_i = \mathbf{e}^i \quad i = 1, \dots, n, \quad (26)$$

where \mathbf{e}_i is the i th unit vector. These systems can be solved quite efficiently using an LU decomposition of A^T (Press et al., 1992).

In the following, Eq. (24) will be evaluated based on different assumptions about the covariance matrix Q of the perturbation vector \mathbf{b} given by

$$Q = \langle \mathbf{b} \mathbf{b}^H \rangle \quad (27)$$

In particular, the extreme cases of perfect correlation and complete decorrelation of the components of \mathbf{b} will be considered.

5. Sensitivity with respect to bathymetry, bottom roughness and wind forcing

In this section the statistical method introduced in the previous section is applied to analyse the sensitivity of the tidal North Sea dynamics with respect to perturbations of the bathymetry, bottom roughness, and wind. The objective is to analyse the respective response patterns and to identify regional differences. The general approach is to introduce perturbations at the smallest resolved scale in the model (i.e., white noise) and to study the respective large scale impact.

5.1. Sensitivity with respect to bathymetry noise

It is well known that there is considerable uncertainty about the bathymetry in the North Sea (Mourre et al., 2004). Very little is known about the spatial distribution of the respective errors, because this involves many factors, like the amount and quality of measurements, or the intensity of morphodynamic processes. We therefore take a very simple approach and assume that the bathymetry h is affected by additive white noise, i.e., h is of the form

$$h = h_0 + \Delta h, \quad (28)$$

where Δh is a zero mean Gaussian process and h_0 is the unperturbed bathymetry. Expanding the bottom roughness terms in Eqs. (13) and (14) to first order, we then have

$$-i \omega \hat{u} - f \hat{v} + g h_0 \frac{\partial \hat{\zeta}}{\partial x} + r_1 \hat{u} / h_0 = \Delta h \left(r_1 \hat{u} / h_0^2 - g \frac{\partial \hat{\zeta}}{\partial x} \right) \quad (29)$$

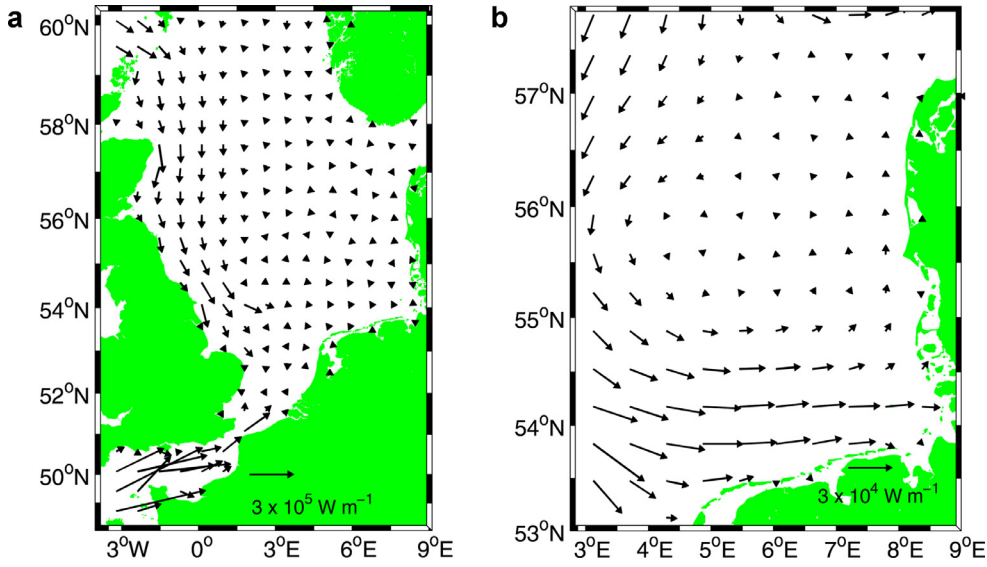


Fig. 6. (a) Energy fluxes estimated with the linear model for the North Sea. (b) Zoom into German Bight with different scaling of arrow lengths.

$$-i \omega \hat{v} + f \hat{u} + gh_0 \frac{\partial \hat{\zeta}}{\partial y} + r_1 \hat{v}/h_0 = \Delta h \left(r_1 \hat{v}/h_0^2 - g \frac{\partial \hat{\zeta}}{\partial y} \right). \quad (30)$$

Denoting the right hand sides for the u and v momentum equations with b^u and b^v , one obtains for each equation

$$\langle |b_k^u|^2 \rangle = \sigma_h^2 \left| r_1 \hat{u}_k/h_k^2 - g \frac{\partial \hat{\zeta}_k}{\partial x} \right|^2 \quad k = 1, \dots, n_{int} \quad (31)$$

$$\langle |b_k^v|^2 \rangle = \sigma_h^2 \left| r_1 \hat{v}_k/h_k^2 - g \frac{\partial \hat{\zeta}_k}{\partial y} \right|^2 \quad k = 1, \dots, n_{int}, \quad (32)$$

where $\sigma_h^2 = \langle \Delta h^2 \rangle$, n_{int} denotes the number of interior points, and $\hat{\zeta}$, \hat{u} , \hat{v} are solutions of the system Eqs. (12)–(14). Eqs. (31), and (32) define the diagonal elements of the matrix Q (see Eq. (27)), which are associated with the interior points. The remaining elements of this matrix are set to zero, because we are considering uncorrelated noise. The statistical approach in Section 4 is then applied. Fig. 7a shows results obtained if a standard deviation (stdv) of 1 m is assumed for the bathymetry noise. One can see that the German Bight stands out with its sensitivity with respect to topography errors. As expected, the shallow areas between the barrier islands and the mainland are particularly strongly affected by this kind of perturbations. The other sensitive areas are the Thames estuary and The Wash bay at the English coast, as well as the Golf de Saint-Malo at the French coast, and the Westerschelde estuary in the Netherlands (south of Zeeland).

5.2. Sensitivity with respect to bottom roughness noise

Let us now assume that the bottom roughness r is affected by additive noise, i.e., we have a perturbed roughness field r_1

$$r_1 = r_0 + \Delta r, \quad (33)$$

where Δr is a zero mean, white Gaussian process and r_0 is the unperturbed roughness field. For the momentum equation we then have

$$-i \omega \hat{u} - f \hat{v} + gh \frac{\partial \hat{\zeta}}{\partial x} + r_0 \hat{u}/h = -\Delta r \hat{u}/h \quad (34)$$

$$-i \omega \hat{v} + f \hat{u} + gh \frac{\partial \hat{\zeta}}{\partial y} + r_0 \hat{v}/h = -\Delta r \hat{v}/h. \quad (35)$$

Denoting the right hand sides for the u and v momentum equations again with b^u and b^v , we get

$$\langle |b_k^u|^2 \rangle = \sigma_r^2 |\hat{u}/h|^2 \quad k = 1, \dots, n_{int}, \quad (36)$$

$$\langle |b_k^v|^2 \rangle = \sigma_r^2 |\hat{v}/h|^2 \quad k = 1, \dots, n_{int}, \quad (37)$$

where $\sigma_r^2 = \langle \Delta r^2 \rangle$, n_{int} is the number of interior grid points, and \hat{u} , \hat{v} are solutions of the system Eqs. (12)–(14). Eqs. (36), and (37) define the diagonal elements of the matrix Q (see Eq. (27)), which are associated with the interior points. As in the previous section, the remaining elements of this matrix are set to zero, because we are considering uncorrelated noise. With this definition the method described in Section 4 is applied. The resulting stdv for the water level is shown in Fig. 7b. As before, the areas south and east of the barrier islands stand out in the German Bight. In addition, we see larger variations inside the English Channel and along the English south east coast. This is consistent with the strong currents and dissipation found in those areas (see Figs. 4 and 5).

The effects of the roughness perturbations on the zonal and meridional currents speeds are shown in 7c, and d. One can see that a region in the English Channel approximately between 2°W and 1°W stands out in both current components. Also in the strait of Dover, along the English south east coast, and in the German Bight stronger impacts on the currents can be found. Compared to the effects on water elevation the current field stdv shows features on smaller spatial scales, i.e., a region with larger current variations can be found over the Dogger Bank (see Fig. 1b). The smoother appearance of the water level standard deviations can be explained by the fact that the roughness perturbations have a very direct effect on the velocities through the momentum equations, whereas the impact on water level variations is more indirect through integration of the continuity equation.

5.3. Impact of the coastal area

In a second set of computations the bathymetry and roughness perturbation were only applied at grid points with distance less than 10 km to the next land point. This was done to study potential large scale impacts of near shore coastal areas separately. The resulting standard deviations for water level as shown in Fig. 8a and b demonstrate that, for the case of bathymetry perturbations, near land points seem to play the most important role, i.e., the

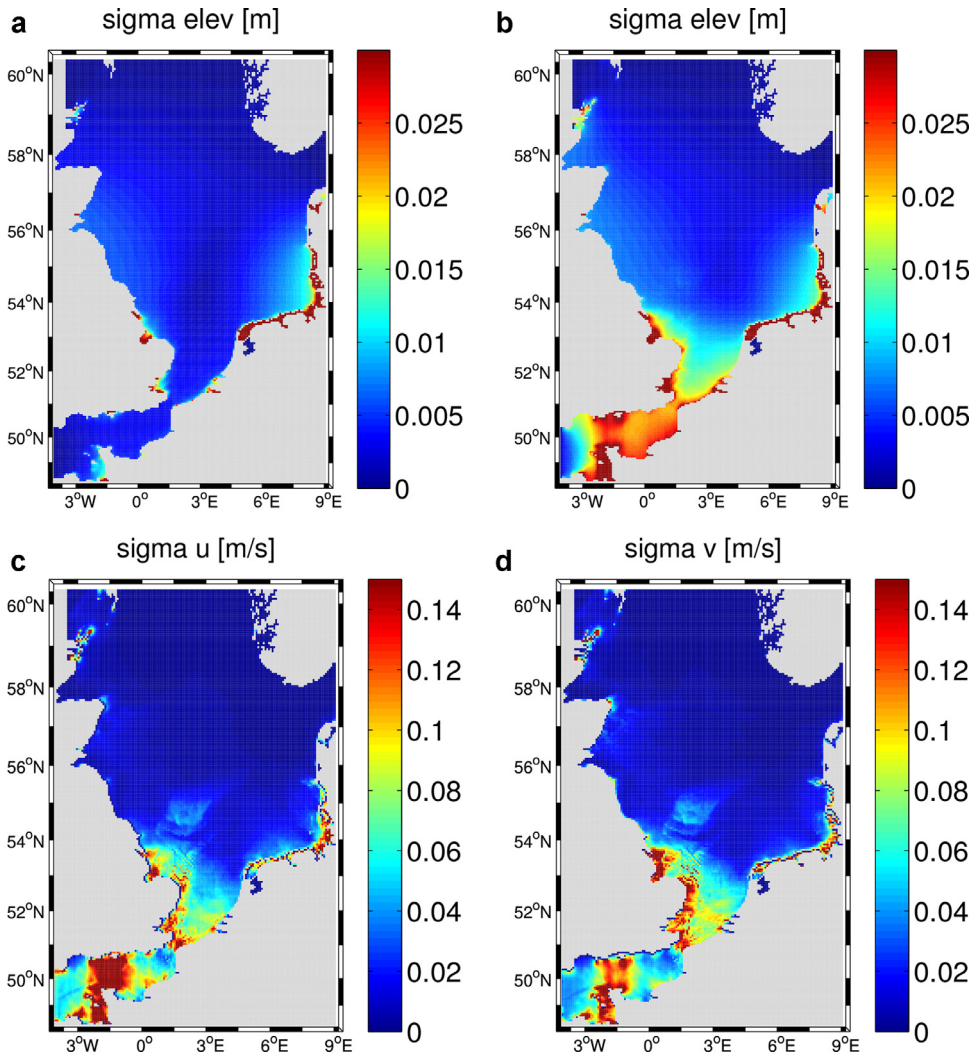


Fig. 7. (a) Standard deviation of water elevation resulting from white noise perturbations of the bathymetry assuming 1 m stdv. (b) Stdv of elevation resulting from white noise perturbations of the bottom friction coefficient r with 50% stdv. (c, d) The same as (b), but for the zonal (c) and meridional (d) current component.

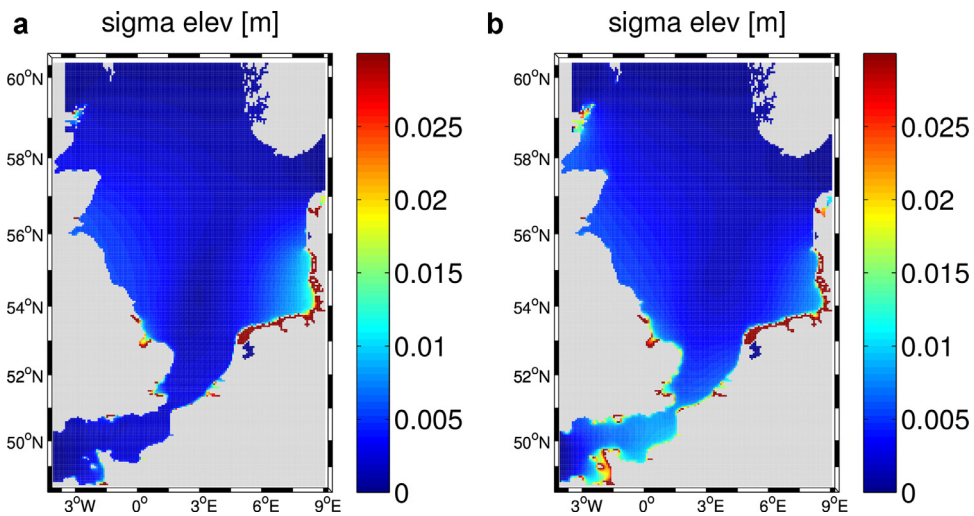


Fig. 8. (a) Standard deviation of water elevation resulting from white noise perturbations of the bathymetry with 1 m stdv within 10 km from land. (b) The same as (a), but for white noise perturbations of the friction coefficient r with 50% stdv.

additional perturbation of grid points further offshore only has a small impact. For the small scale modifications of the roughness parameter larger differences are found. In particular, in the English Channel and along the English south east coast the roughness of grid points farther offshore is of stronger relevance.

5.4. Sensitivity with respect to meteo forcing

In a third set of experiments it was assumed that the main model error source is from the meteo forcing. For this case the linear system Eq. (15) was solved for both the semi-diurnal M2 component and the diurnal S1 component. The correlation between the meridional and zonal wind component was assumed to be zero. Fig. 9 shows results with error stdv of $1 \text{ m}^2 \text{ s}^{-2}$ for the surface friction term. The results for M2 are shown at the top (Fig. 9a, and b) and the results for S1 at the bottom (Fig. 9c, and d). Plots on the left (Fig. 9a, and c) refer to the case with meteo errors fully correlated in space and plots on the right (Fig. 9b, and d) represent the situation with white noise errors. As one can see, there are only small differences between M2 and S1 for fully uncorrelated errors. In both cases the largest impacts are found in the very shallow areas along the Dutch, German and Danish coast, as well as in the river Thames estuary and The Wash bay. For fully correlated wind errors the spatial patterns of the resulting stdv of water level amplitudes are very different for both spectral components. For the M2 tide a maximum can be found in the German Bight and along the English north east coast. For the S1 tide the strongest impact is seen in front of the English Channel and the English south east coast. It has to be emphasized that again clamped conditions were used for the open boundaries, i.e., the wind perturbations are allowed to act only locally inside the North Sea. This means that the waves generated by the wind are trapped and the response patterns are strongly influenced by the boundary conditions and the respective wavelength. One can see that the response pattern for S1 shows a larger correlation length than the one for M2. In particular, we have three maxima for M2 and only two maxima for S1. This is due to the fact that shallow water waves with semi-diurnal frequency have half the wavelength of those with diurnal frequency.

6. Perturbations along the nested model boundary

The sensitivity analysis presented in this section is based on the assumption that the German Bight model is nested into the North Sea model. The respective model domains are depicted in Fig. 1. Bathymetries for both model grids are shown in Fig. 2.

We further assume that within this smaller region modification of the dynamics are applied, e.g., by

- running an assimilation system,
- changing model parameters like for example roughness or bathymetry.

In a two-way nested model system these changes are fed back into the larger North Sea model through the respective boundary. The impact of these perturbations on the North Sea model is analysed below by introducing the German Bight boundaries as new open boundaries into the larger model. For the reference run the respective boundary values were again taken from the operational BSH model.

The statistical approach introduced in Section 4 is applied as follows. Assuming that the boundary forcing perturbations are uncorrelated, one can reorder the equations in the linear system Eq. (15) such that $\langle \mathbf{b}\mathbf{b}^H \rangle$ can be written as

$$\langle \mathbf{b}\mathbf{b}^H \rangle = \sigma_{ob}^2 \begin{pmatrix} I_{n_{ob}} & 0 \\ 0 & 0 \end{pmatrix}, \quad (38)$$

where n_{ob} is the number of forced points along the German Bight boundary and $I_{n_{ob}}$ is the identity matrix of dimension n_{ob} . One can imagine these uncorrelated perturbations, for example, to be small scale corrections coming from observations inside the German Bight with high spatial resolution, e.g., from an HF radar (Paduan and Washburn, 2012; Stanev et al., 2015).

For the case where the boundary perturbations are fully correlated we have

$$\langle \mathbf{b}\mathbf{b}^H \rangle = \sigma_{ob}^2 \begin{pmatrix} O_{n_{ob}} & 0 \\ 0 & 0 \end{pmatrix}, \quad (39)$$

where $O_{n_{ob}}$ is an $n_{ob} \times n_{ob}$ matrix filled with ones. In this case one can imagine these perturbation as large scale corrections of the tidal dynamics inside the German Bight, e.g., adjustments of the timing or amplitude of the tidal wave.

6.1. Experiments with clamped condition at North Sea open boundary

Fig. 10 shows the resulting standard deviations for the water level assuming that the perturbations at the open boundary have a stdv of 0.3 m. For the case with uncorrelated perturbations shown in Fig. 10a one can see that strong impacts can only be found in the direct vicinity of the open boundary. There are some far field effects seen along the English east coast, but with less than 30% stdv of the original perturbations these are relatively weak. Fig. 10b shows the other extreme case of fully correlated perturbations with 0.3 m stdv. In this case we see a much stronger impact both in the vicinity of the open boundary and at the English east coast. The introduced variations along the English coast are about as big as the original perturbation at the German Bight boundary.

The qualitative structure of the responses found for the North Sea system are not surprising, because in the case of correlated noise a much more coherent and focused signal is introduced, which can be expected to have a larger impact than uncorrelated noise, which diffuses much quicker. Correlated perturbations are more effective in generating large scale M2 eigenmodes of the North Sea system. However, the large magnitude of the response found at the English coast deserves some further analysis. The key point to take into account here is that the introduced perturbations cannot propagate freely, because the original forcing for the open boundaries in the English Channel, in the north, and towards the Baltic Sea are still used for the North Sea model. This means that the estimated responses have to compensate the introduced perturbations in such a way that the water elevations remain the same at these boundaries.

6.2. Experiments with radiation condition at the North Sea open boundary

To get a better a picture how the perturbations along the German Bight open boundary propagate freely inside the North Sea, another experiment was performed using radiation boundary conditions for the remaining boundaries. The radiation boundary condition for a wave leaving the domain in positive x direction reads

$$\frac{\partial \zeta}{\partial t} = -\sqrt{gh} \frac{\partial \zeta}{\partial x} \quad (40)$$

with water depth h and gravitational acceleration g . Using the spectral representation Eq. (11) this can be expressed as

$$-i\omega \hat{\zeta} = -\sqrt{gh} \frac{\partial \hat{\zeta}}{\partial x}, \quad (41)$$

which can be easily integrated into the linear system Eq. (15).

Fig. 10c shows the respective water level stdv resulting from fully correlated perturbations along the German Bight open boundary with 0.3 m stdv. Comparing this result to Fig. 10b shows that

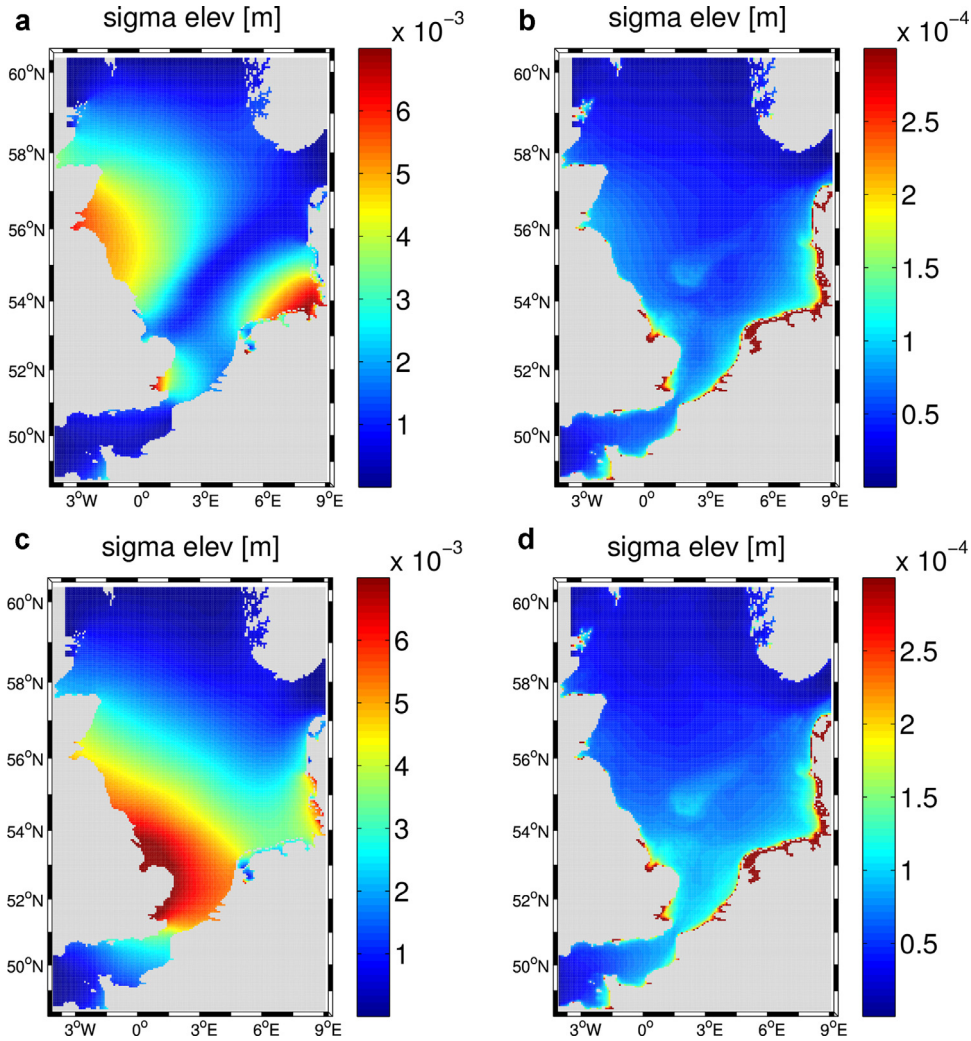


Fig. 9. (a) Standard deviation of elevation resulting from wind perturbations with M2 periodicity assuming perfect spatial correlation for the u and v component. The correlation between both wind components is assumed to be zero. (b) The same as (a), but assuming complete spatial decorrelation of wind perturbations. (c, d) The same as (a, b) but for daily cycle S1.

the far field effect at the English coast, while still being significant, is strongly reduced in this case. The near field impact radius, on the other hand, is slightly extended in the westerly direction.

There is one immediate lesson to be learned from this result. Running an assimilation system for the North Sea with observations in the German Bight one has two basic options for the treatment of the open boundary forcing for the North Sea model in the English Channel and at the northern boundary.

- One can assume that the open boundary forcing along these boundaries is correct in the free run and thus keep them unchanged.
- One can let the correction signal being applied by the analysis scheme in the German Bight radiate out of the North Sea area, which will then change the state estimates also along the western and northern open boundaries.

As shown above the first approach will lead to somehow artificial compensation signals inside the North Sea. The second approach will of course lead to inconsistencies between the North Atlantic model and the North Sea model, unless an upscaling approach is also taken for these models. One approach, where the North Sea open boundary forcing is adjusted using an ensemble method, is described in Barth et al. (2010). Depending on the application one has to choose, which approach to take.

7. Linear solution for a nested setup

Here, we consider a two way coupled North Sea/German Bight model. The North Sea model is run on the same grid as in the previous experiments (see Fig. 2a). For the German Bight a finer grid with 1 km resolution is used (see Fig. 2b).

As done before, the German Bight area is removed from the coarse North Sea model, and an additional open boundary is introduced along the German Bight boundary. We then have to solve the linear system Eq. (15) for both domains, i.e., we have two systems of the form

$$A_{ns} \mathbf{x}_{ns} = \mathbf{b}_{ns} \tag{42}$$

$$A_{gb} \mathbf{x}_{gb} = \mathbf{b}_{gb}, \tag{43}$$

where the indices “ns” and “gb” stand for North Sea and German Bight, respectively. The right hand side vectors are split into

$$\mathbf{b}_{ns} = \begin{pmatrix} \hat{\mathbf{b}}_{ns} \\ \tilde{\mathbf{b}}_{ns} \end{pmatrix} \quad \text{and} \quad \mathbf{b}_{gb} = \begin{pmatrix} \hat{\mathbf{b}}_{gb} \\ \tilde{\mathbf{b}}_{gb} \end{pmatrix}, \tag{44}$$

where $\hat{\mathbf{b}}_{ns}$, $\hat{\mathbf{b}}_{gb}$ correspond to the clamped boundary forcing points along the German Bight and $\tilde{\mathbf{b}}_{ns}$, $\tilde{\mathbf{b}}_{gb}$ are the remaining components of the right hand side vectors. To obtain this form the equations in

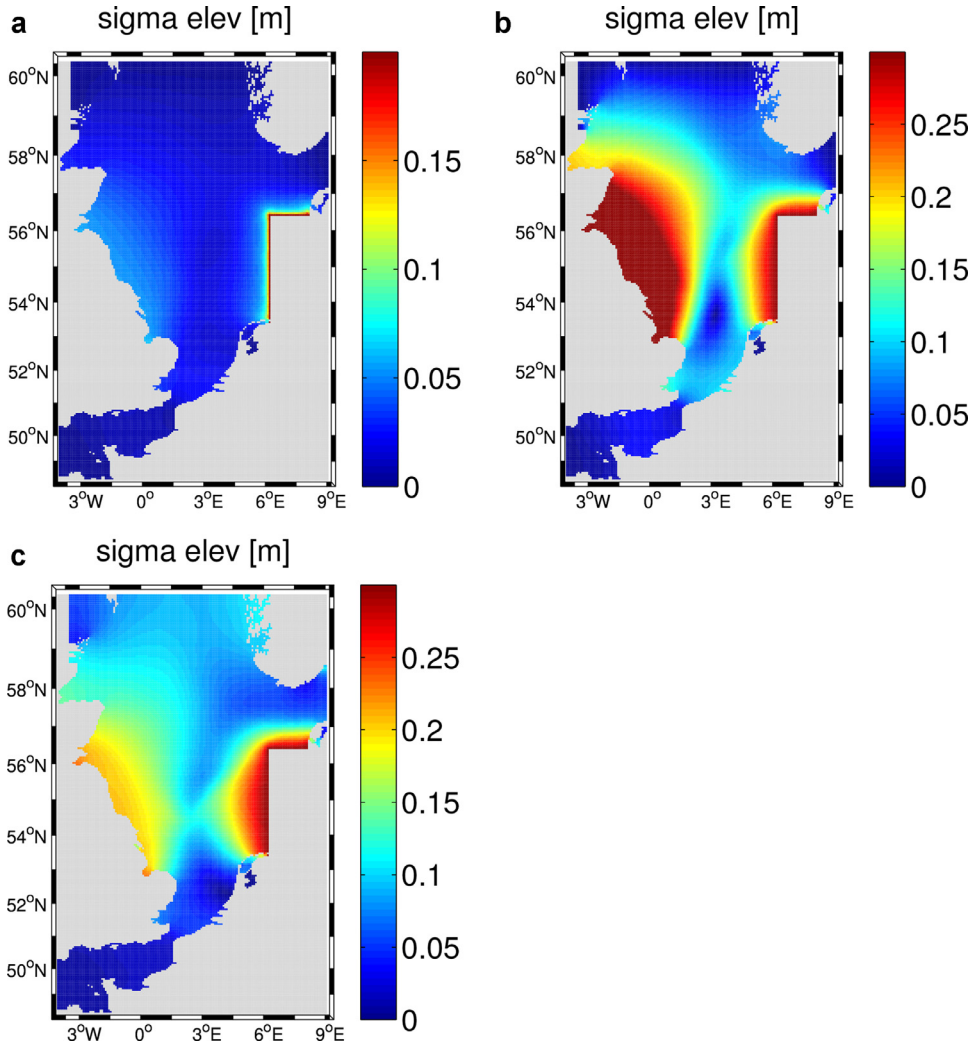


Fig. 10. Standard deviation of elevation resulting from white noise perturbations (a) and fully correlation perturbations (b) with stdv 0.3 m along the German Bight border. (c) The same as (b), but using radiation boundary conditions for the remaining open boundaries of the North Sea model.

the linear systems Eqs. (42) and (43) may have to be reordered accordingly. The right hand sides $\hat{\mathbf{b}}_{ns}$ and $\hat{\mathbf{b}}_{gb}$ are connected via

$$\hat{T}_\eta \hat{\mathbf{b}}_{ns} = \hat{\mathbf{b}}_{gb}, \quad (45)$$

where the linear operator \hat{T}_η translates the coarse clamped boundary forcing of the North Sea model to the fine resolution boundary forcing of the German Bight model using linear interpolation. For a given boundary forcing along the German Bight boundary the solutions can then be written as

$$\mathbf{x}_{ns} = \hat{A}_{ns}^{-1} \hat{\mathbf{b}}_{ns} + \tilde{A}_{ns}^{-1} \tilde{\mathbf{b}}_{ns} \quad (46)$$

$$\mathbf{x}_{gb} = \hat{A}_{gb}^{-1} \hat{\mathbf{b}}_{ns} + \tilde{A}_{gb}^{-1} \tilde{\mathbf{b}}_{gb}. \quad (47)$$

Here, the matrices $\hat{A}_{ns}^{-1}, \hat{A}_{gb}^{-1}, \tilde{A}_{ns}^{-1}, \tilde{A}_{gb}^{-1}$ contain columns of the matrices A_{ns}^{-1}, A_{gb}^{-1} associated with the German Bight open boundary points and the remaining points, respectively, i.e.,

$$A_{ns}^{-1} = (\hat{A}_{ns}^{-1}, \tilde{A}_{ns}^{-1}) \quad (48)$$

$$A_{gb}^{-1} = (\hat{A}_{gb}^{-1}, \tilde{A}_{gb}^{-1}). \quad (49)$$

In order to be consistent, not only the elevations, but also the transports across the German Bight boundary have to match.

In general, for some given clamped forcing at the German Bight boundary the German Bight model and the North Sea model will respond with different currents at this boundary. The idea is to choose the clamped forcing such that the resulting transports are the same for both domains. For the linear model this constraint leads to a simple linear system of equations as explained in the following. Let us denote by T_{ns} the operator which extracts the transports across the open boundary from the North Sea model state vector \mathbf{x}_{ns} and by T_{gb} the operator, which extracts the transports across the open boundary from the German model state vector \mathbf{x}_{gb} . The operator T_{gb} furthermore translates the fine GB grid to the coarser NS grid by averaging. We then require

$$T_{ns} \hat{A}_{ns}^{-1} \hat{\mathbf{b}}_{ns} + T_{ns} \tilde{A}_{ns}^{-1} \tilde{\mathbf{b}}_{ns} = T_{gb} \hat{A}_{gb}^{-1} \hat{T}_\eta \hat{\mathbf{b}}_{ns} + T_{gb} \tilde{A}_{gb}^{-1} \tilde{\mathbf{b}}_{gb} \quad (50)$$

and hence, we get the following linear system of equations to be solved for the boundary forcing in the coarse grid model $\hat{\mathbf{b}}_{ns}$:

$$(T_{ns} \hat{A}_{ns}^{-1} - T_{gb} \hat{A}_{gb}^{-1} \hat{T}_\eta) \hat{\mathbf{b}}_{ns} = T_{gb} \tilde{A}_{gb}^{-1} \tilde{\mathbf{b}}_{gb} - T_{ns} \tilde{A}_{ns}^{-1} \tilde{\mathbf{b}}_{ns} \quad (51)$$

The forcing for the German Bight model then follows from Eq. (45). The solution of the system Eq. (51) ensures that both the elevation and the currents match along the boundary between both model domains. The dimension of the system is equal to the relatively small number of boundary points and hence, standard solvers for general complex matrices can be used. The real

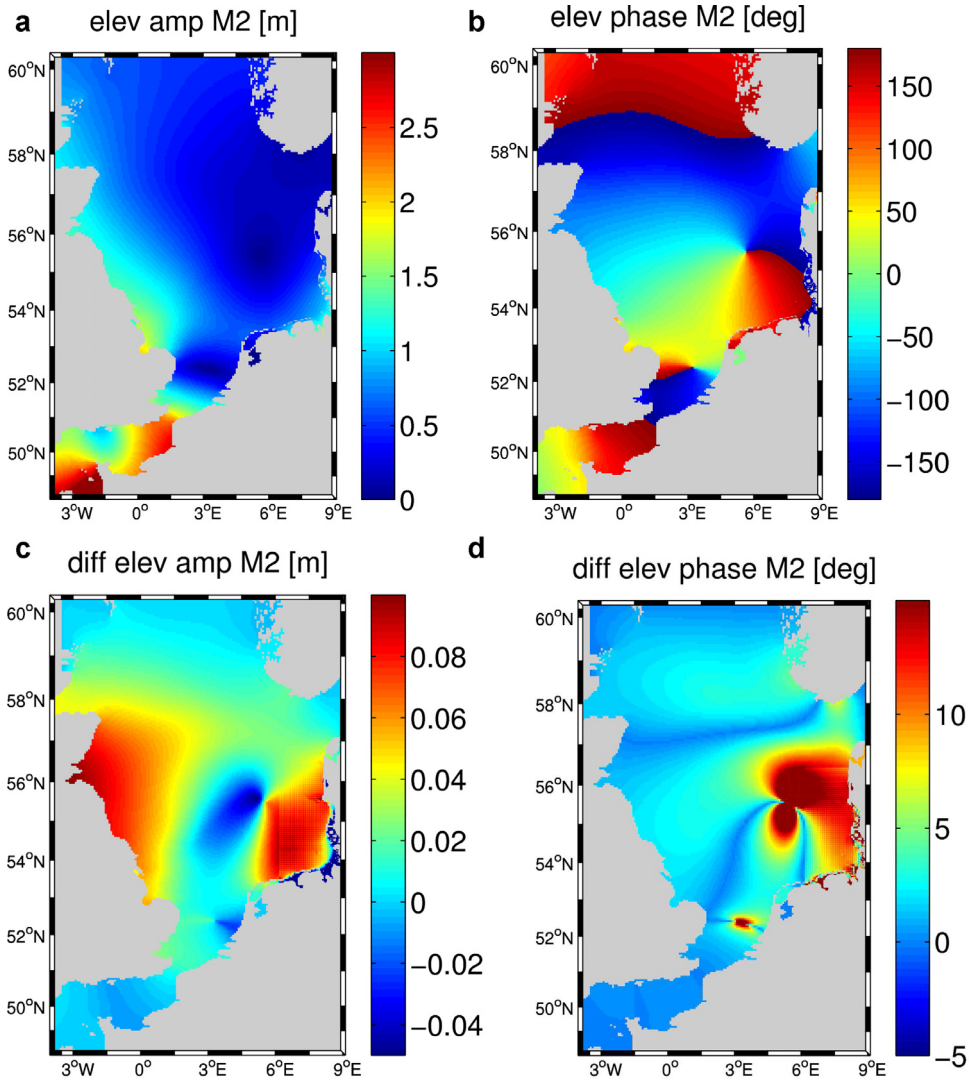


Fig. 11. (a, b) M2 elevation amplitude (a) and phase (b) of the nested setup. (c, d) Difference of the M2 elevation amplitude (c) and phase (d) of the coarse setup and the nested setup.

computational effort lies in the formation of the matrix in brackets and the right hand side.

Fig. 11a and b shows the M2 amplitudes and phases for the nested model setup. The amplitude and phase differences with respect to the previous model run with coarse German Bight bathymetry (see Fig. 3) are presented in Fig. 11c and d. As one can see, the higher resolution in the German Bight area leads to amplitude changes up to 10 cm not only inside this region, but there are also far field effects visible along the English east coast. The impact on the M2 phase is concentrated in the high resolution grid area and around the amphidromic points with phase differences up to 20°, which corresponds to 40 min time lag.

8. Kalman analysis using observations

In this section we will study the impact of observations acquired in a coastal area on the regional scale making different assumptions about the type of model error. These kind of studies are usually referred to in literature as Observing System Experiments (OSE's) and Observing System Simulation Experiments (OSSE's) (Le Hénaff et al., 2009; Schulz-Stellenfleth and Stanev, 2010; Sakov and Oke, 2008).

Following the standard statistical approach, we assume that the model errors follow a zero mean Gaussian distribution with covariance matrix P . Furthermore, the observation vector \mathbf{y}_{obs} and the state vector \mathbf{x} are connected via

$$\mathbf{y}_{obs} = H\mathbf{x} + \epsilon, \tag{52}$$

where H is the observation operator and ϵ is a zero mean Gaussian process with covariance matrix G . For a given measurement vector y_{obs} and a first guess state \mathbf{x}_f the analysed state vector \mathbf{x}_a can then be computed according to the following Kalman equation:

$$\mathbf{x}_a = \mathbf{x}_f + K(\mathbf{y}_{obs} - H\mathbf{x}_f) \tag{53}$$

with the Kalman gain matrix

$$K = P H^T (H P H^T + G)^{-1}. \tag{54}$$

The covariance matrix of the analysed state then follows as (e.g. Evensen, 2006):

$$P_a = P - P H^T (H P H^T + G)^{-1} H P. \tag{55}$$

In the standard formulation these equations refer to real valued vectors. For the application of the Kalman analysis we therefore switch from the complex notation used in the previous chapters to

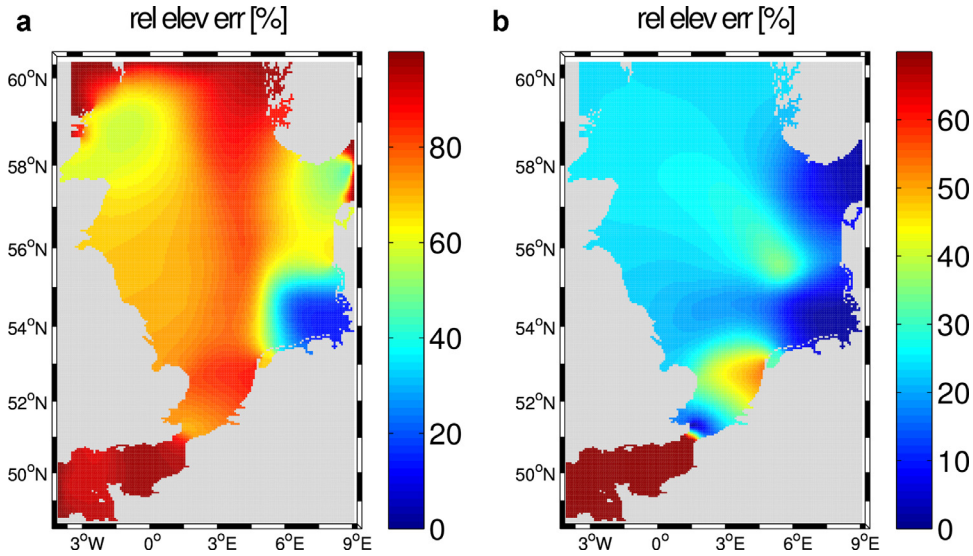


Fig. 12. Normalised analysis error of the M2 water level resulting from a single tide gauge measurement in the German Bight (8.0°E 54.0°N) with 0.01 m accuracy. The source of the model error is assumed to be white noise (a) and fully correlated noise (b) added to the water level at the open boundaries of the North Sea model with 0.5 m stdv.

real values, i.e., we define a new state vector $\tilde{\mathbf{x}}$ and a new observation vector $\tilde{\mathbf{y}}$ as

$$\tilde{\mathbf{x}} = (\text{Re}(\mathbf{x}), \text{Im}(\mathbf{x})) \quad (56)$$

$$\tilde{\mathbf{y}} = (\text{Re}(\mathbf{y}_{obs}), \text{Im}(\mathbf{y}_{obs})), \quad (57)$$

where Re and Im denote the real and imaginary part of complex numbers. The augmented observation operator matrix \tilde{H} of dimension $2n \times 2n_{obs}$ is given accordingly as

$$\tilde{H} = \begin{pmatrix} H & 0 \\ 0 & H \end{pmatrix}, \quad (58)$$

where we have used that only real valued observation operators are considered in this study.

The covariance matrix of the real state vector then reads

$$P_{\tilde{\mathbf{x}}} = \frac{1}{2} \begin{pmatrix} \text{Re}(P_x + P_x^{\xi}) & \text{Im}(-P_x + P_x^{\xi}) \\ \text{Im}(P_x + P_x^{\xi}) & \text{Re}(P_x - P_x^{\xi}) \end{pmatrix}, \quad (59)$$

where we used the definitions

$$P_x = \langle \mathbf{x}\mathbf{x}^H \rangle \quad (60)$$

$$P_x^{\xi} = \langle \mathbf{x}\mathbf{x}^T \rangle \quad (61)$$

with the complex covariance function P_x , the pseudo-covariance function P_x^{ξ} (Goh and Mandic, 2007), and the superscript T indicating matrix transpose. For the perturbations of the right hand side vector \mathbf{b} discussed in the previous sections one obtains

$$P_x = \hat{A} \langle \mathbf{b}\mathbf{b}^H \rangle \hat{A}^H \quad (62)$$

$$P_x^{\xi} = \hat{A} \langle \mathbf{b}\mathbf{b}^T \rangle \hat{A}^T, \quad (63)$$

where we have used the definition $\hat{A} = A^{-1}$ to simplify the notation. The real covariance matrix $P_{\tilde{\mathbf{x}}}$ in Eq. (59) can then be readily computed.

Because of the large dimension, the computations were done on a linux cluster using the MPI library. Again, we avoided the storage of the complete matrix A^{-1} . In a first step the matrix HA^{-1} was computed. The required columns of A^{-1} were obtained on the fly from the LU decomposition of A similar to the approach described

in the last section. Subsequently, the matrix $HP_{\tilde{\mathbf{x}}}$ can be computed as

$$\tilde{H}P_{\tilde{\mathbf{x}}} = \frac{1}{2} \begin{pmatrix} \text{Re}(H\hat{A}Q(\hat{A}^H + \hat{A}^T)) & -\text{Im}(H\hat{A}Q(\hat{A}^H + \hat{A}^T)) \\ \text{Im}(H\hat{A}Q(\hat{A}^H + \hat{A}^T)) & \text{Re}(H\hat{A}Q(\hat{A}^H - \hat{A}^T)) \end{pmatrix}, \quad (64)$$

where we have again used that H is a real valued operator. Having the matrix HP available, the expression for the posterior covariance matrix defined in Eq. (55) was evaluated step by step, starting with the matrix in brackets.

In the following an experiment is described, in which the impact of a single tide gauge measurement in the German Bight is analysed considering different types of model errors. Fig. 12 shows relative standard deviations of the analysis in per cent with respect to the background standard deviations given by the matrix P . In this case water level measurements are assumed to be taken at a single location in the German Bight (8.0°E 54.0°N) with 0.01 m accuracy. Fig. 12a refers to the situation where the model errors are caused by white noise at the open boundaries of the North Sea grid, whereas (b) represents the case where the error sources at the boundary are fully correlated. In both cases the errors are assumed to have a stdv of 0.5 m. One can see that the error reduction achieved by using the observations is quite restricted to the German Bight area for the case of uncorrelated forcing errors. This is not surprising, because the spatial error patterns inside the North Sea caused by the uncorrelated boundary forcing errors can be expected to have a short correlation length and thus the information from measurements cannot spread very far. For the case with fully correlated errors shown in Fig. 12b one can see that observations taken at a single location can make a big difference. In this situation only the state estimates inside the English Channel are not significantly improved by the observations.

9. Summary and conclusions

In this study the impact of different types of small scale perturbations on larger scales was investigated for the two-dimensional barotropic dynamics of the North Sea. The investigation was motivated by recent developments concerning the availability of operational regional models and observations from coastal observatories.

A linear model was used for the analysis, which allowed a rigorous statistical analysis without the need of Monte Carlo

simulations. The Navier Stokes equations were solved in the spectral domain and it was demonstrated that the main dynamical features of the fully nonlinear 3D model, which was used to provide forcing data at the open boundaries, are well captured by this approach. A North Sea grid with 5 km resolution and a German Bight grid with 1 km resolution was used for the analysis.

In the first experiment white noise was added to the bathymetry and the bottom roughness in the entire North Sea. It was found that the German Bight stands out with the highest sensitivity to bathymetry uncertainties. This can be attributed to the small water depth in that area. The uncertainties of bottom roughness were shown to have strong impacts in the English Channel and along the south east coast of England. The Wadden Sea areas between the barrier islands and the mainland in the German Bight were strongly affected by roughness perturbations as well. This is again due to the very shallow water in that area. The high sensitivity in the English Channel is associated with strong currents in the region. In another experiment the perturbations were restricted to grid points with less than 10 km distance to land. It was shown that these near land points are the most critical ones with regard to bathymetry uncertainties. For bottom roughness perturbations areas further offshore are of importance as well. Noise was then added to the diurnal and semidiurnal components of the wind forcing. It was shown that in case of white noise the impact is restricted to the very shallow areas in particular along the barrier islands. For fully correlated wind perturbations large scale impacts can be found, which are significantly different for the M2 and S1 frequency components.

In the second set of experiments a new open boundary was introduced along the German Bight boundary. Perturbations were then applied to the respective forcing. The motivation for this approach was to study potential impacts of perturbations inside the German Bight area on the North Sea. These perturbations could, for example, originate from a coastal data assimilation system or from modifications of model parameters inside the coastal area. It was shown that the impact strongly depends on the correlation properties of the perturbations. In case of strong correlations a significant far field effect was found leading to a stronger impact along the east coast of England. It was furthermore shown that this far field effect is very dependent on the type of boundary condition used for the North Sea model. Introducing a radiation boundary condition along the English Channel, the northern boundary and the Skagerrak leads to a significant reduction of the far field effect. In this case the perturbations created along the German Bight boundary can radiate out of the North Sea domain and are not reflected back, as in the previous experiment with clamped boundary conditions.

In a second step, a German Bight grid with 1 km resolution was nested into the North Sea grid. An approach was presented to solve the linear Navier Stokes equations in a two-way coupled setup using a spectral approach. Results obtained with the nested configuration and the original 5 km setup were compared in terms of M2 phases and amplitudes. Amplitude differences of up to 10 cm and phase differences of up to 20° were observed. The impact on M2 amplitudes was not restricted to the German Bight, but a significant far field effect could be observed along the English east coast.

Finally, the impact of water level measurements taken in the German Bight was analysed based on different assumptions about the type of model errors. For this purpose the Kalman analysis equation was evaluated using different formulations for the model error covariance matrix. It was shown that the observations are most effective in case of correlated errors of the open boundary forcing. In this case the information gathered by the observation instruments is spread far beyond the boundaries of the German Bight. If the model errors are spatially uncorrelated the influence

radius of measurements taken at a single location is smaller, but can still cover the entire German Bight.

It was pointed out at the beginning that the definition of upscaling is not straightforward and different research groups seem to use the term in quite different contexts. In this study we have used the terminology analysing the interplay of coastal and regional scales. Different aspects like model nesting, small scale perturbations, or impact of coastal observations were investigated. The study has shown that the coupling of coastal and regional models using downscaling approaches is not sufficient in the long run. This point is of particular concern when observations are assimilated into nested model systems. One-way downscaling techniques are traditionally used because of their ease of implementation. However, the sophistication of ocean models has reached a level where upscaling mechanisms cannot be neglected any more. For example, a lot work has been done on the integration of coupling mechanisms between currents, ocean waves, and atmosphere into models. These mechanisms lead to an energy and momentum transfer between different spatial scales and inappropriate nesting techniques can lead to significant artefacts. It is furthermore obvious that cross-border advection processes cannot be treated optimally in a one-way nested setup. Also, there is a growing amount of high resolution information available on the coastal scale, e.g., from coastal observations or hydrological models, which cannot be fed into a regional model directly, because essential processes are not resolved. The most obvious way to make best use of such data is the implementation of upscaling techniques. In general, there is growing demand for ocean information, which is dynamically consistent on different scales. This is an important issue for both climate studies and operational forecast systems. More work has to be done on the development of efficient and flexible two-way nesting techniques as well as suitable data assimilation methods. It can be foreseen that with the growing number of coastal observatories and the growing sophistication of multi-scale modelling approaches the upscaling issue will be of increasing importance in the future.

Acknowledgements

The presented work was supported by the European Research Council in the framework of the [Seventh Framework Program](#) projects MYOCEAN-2 (Grant agreement no. [283367](#)) and JERICO (Grant agreement no. [123456](#)). We also thank the BSH for providing numerical model data.

References

- Andersen, O.B., Egbert, G.D., Erofeeva, S.Y., Ray, R.D., 2006. Mapping nonlinear shallow-water tides: a look at the past and future. *Ocean Dyn.* 56 (5–6), 416–429. doi:[10.1007/s10236-006-0060-7](#).
- Backhaus, J., 1976. Zur Hydrodynamik im Flachwassergebiet. Ein numerisches Modell. *Dtsch. Hydrogr. Z.* 6, 222–238. doi:[10.1007/BF02226256](#).
- Barth, A., Alvera-Azcárate, A., Beckers, J.M., Weisberg, R.H., Vandenbulcke, L., Lenartz, F., Rixen, M., 2009. Dynamically constrained ensemble perturbations: application to tides on the west florida shelf. *Ocean Sci.* 5, 259–270.
- Barth, A., Alvera-Azcárate, A., Gurgel, K.-W., Staneva, J., Port, A., Beckers, J.-M., Stanev, E., 2010. Ensemble perturbation smoother for optimizing tidal boundary conditions by assimilation of high-Frequency radar surface currents – application to the German Bight. *Ocean Sci.* 6, 161–178. doi:[10.5194/os-6-161-2010](#).
- Barth, A., Alvera-Azcárate, A., Rixen, M., Beckers, J.-M., 2005. Two-way nested model of mesoscale circulation features in the Ligurian Sea. *Prog. Oceanogr.* 66 (2), 171–189. doi:[10.1016/j.pocan.2004.07.017](#).
- Bolaños, R., Jordá, G., Cateura, J., Lopez, J., Puigdefabregas, J., Gómez, J., Espino, M., 2009. The XIOM: 20 years of a regional coastal observatory in the Spanish Catalan coast. *J. Mar. Syst.* 77 (3), 237–260. doi:[10.1016/j.jmarsys.2007.12.018](#).
- Davies, A.M., Kwong, S., 2000. Tidal energy fluxes and dissipation on the European continental shelf. *J. Geophys. Res.* (1978–2012) 105 (C9), 21969–21989. doi:[10.1029/2000JC900078](#).
- Di Lorenzo, E., Moore, A., Arango, H., Cornuelle, B., Miller, A., B, P., Chua, B., Bennett, A., 2007. Weak and strong constraint data assimilation in the inverse regional ocean modeling system (ROMS): development and application for a baroclinic coastal upwelling system. *Ocean Modell.* 16, 160–187. doi:[10.1016/j.oceanmod.2006.08.002](#).

- Dick, S., Kleine, E., Müller-Navarra, S.H., Klein, H., Komo, H., 2001. The Operational Circulation Model of BSH (BSHcmod): Model Description and Validation. Technical Report 29. BSH.
- Evensen, G., 2006. *Data Assimilation: The Ensemble Kalman Filter*. Springer, Berlin.
- Goh, S.L., Mandic, D.P., 2007. An augmented extended Kalman filter algorithm for complex-valued recurrent neural networks. *Neural Comput.* 19 (4), 1039–1055. doi:10.1029/2000JC900078.
- Hashemi, M.R., Neill, S.P., Davies, A.G., 2014. A coupled tide-wave model for the NW European shelf seas. *Geophys. Astrophys. Fluid Dyn.* 109, 234–253. ahead-of-print. doi:10.1080/03091929.2014.944909.
- Hasselmann, K., 1976. Stochastic climate models, Part I. Theory. *Tellus A* 28 (6), 473–485.
- Howarth, J., Palmer, M., 2011. The Liverpool bay coastal observatory. *Ocean Dyn.* 61 (11), 1917–1926. doi:10.1007/s10236-011-0458-8.
- Kourafalou, V., De Mey, P., Le Hénaff, M., Charria, G., Edwards, C., He, R., Herzfeld, M., Pascual, A., Stanev, E., Tintoré, J., others, 2015. Coastal ocean forecasting: system integration and evaluation. *J. Oper. Oceanogr.* 8 (Suppl. 1), S127–S146. doi:10.1080/1755876X.2015.1022336.
- Kraichnan, R.H., 1967. Inertial ranges in two-dimensional turbulence. *Phys. Fluids* 10 (7), 1417–1423. doi:10.1063/1.1762301.
- Le Hénaff, M., De Mey, P., Marsaleix, P., 2009. Assessment of observational networks with the representer matrix spectra method – application to a 3d coastal model of the Bay of Biscay. *Ocean Dyn.* 59, 3–20. doi:10.1007/s10236-008-0144-7.
- Maier-Reimer, E., 1977. Residual circulation in the North Sea due to the M2 tide and mean annual wind stress. *Ocean Dyn.* 30, 69–80. doi:10.1007/BF02226256.
- Merckelbach, L., 2013. On the probability of underwater glider loss due to collision with a ship. *J. Mar. Sci. Technol.* 18 (1), 75–86. doi:10.1007/s00773-012-0189-7.
- Moore, A.M., Arango, H.G., Di Lorenzo, E., Cornuelle, B.D., Miller, A.J., Neilson, D.J., 2004. A comprehensive ocean prediction and analysis system based on the tangent linear and adjoint of a regional ocean model. *Ocean Modell.* 7 (1), 227–258. doi:10.1016/j.ocemod.2003.11.001.
- Moore, A.M., Arango, H.G., Di Lorenzo, E., Miller, A.J., Cornuelle, B.D., 2009. An adjoint sensitivity analysis of the Southern California Current circulation and ecosystem. *J. Phys. Oceanogr.* 39 (3), 702–720. doi:10.1175/2008JPO3740.1.
- Mourre, B., De Mey, P., Lyard, F., Le Provost, C., 2004. Assimilation of sea level data over continental shelves: an ensemble method for the exploration of model errors due to uncertainties in bathymetry. *Dyn. Atmos. Oceans* 38, 93–121. doi:10.1016/j.dynatmoce.2004.09.001.
- Munk, W., 1997. Once again: once again—tidal friction. *Prog. Oceanogr.* 40 (1), 7–35. doi:10.1016/S0079-6611(97)00021-9.
- Nastrom, G., Gage, K., Jasperson, W., 1984. Kinetic energy spectrum of large- and mesoscale atmospheric processes. *Nature* 310 (5972), 36–38. doi:10.1038/310036a0.
- Otto, L., Zimmerman, J., Furnes, G., Mork, M., Saetre, R., Becker, G., 1990. Review of the physical oceanography of the North Sea. *Neth. J. Sea Res.* 26 (2), 161–238. doi:10.1016/0077-7579(90)90091-T.
- Paduan, J.D., Washburn, L., 2012. High-frequency radar observations of ocean surface currents. *Annu. Rev. Mar. Sci.* 5, 115–136. doi:10.1146/annurev-marine-121211-172315.
- Press, W.H., Teukolsky, S.A., Vetterling, W.T., Flannery, B.P., 1992. *Numerical Recipes in FORTRAN: The Art of Scientific Computing*. Cambridge University Press, New York.
- Provost, C.L., Rougier, G., Poncet, A., 1981. Numerical modeling of the harmonic constituents of the tides, with application to the English Channel. *J. Phys. Oceanogr.* 11 (8), 1123–1138. doi:10.1175/1520-0485(1981)011(1123:NMOTH)2.0.CO;2.
- Pugh, D.T., 1996. *Tides, Surges and Mean Sea-Level* (reprinted with corrections). John Wiley & Sons Ltd. URL: <http://eprints.soton.ac.uk/id/eprint/19157>
- Riethmüller, R., Colijn, F., Krasemann, H., Schroeder, F., Ziemer, F., 2009. COSYNA, an integrated coastal observation system for the North and Arctic Seas. In: *Proceedings of OCEANS 2009 – Europe*. IEEE, pp. 1–7.
- Sakov, P., Oke, P., 2008. Objective array design: application to the tropical Indian Ocean. *J. Atmos. Ocean. Technol.* 25, 794–807. doi:10.1175/2007JTECHO553.1.
- Schulz-Stellenfleth, J., Stanev, E., 2010. Statistical assessment of ocean observing networks – a study of water level measurements in the German Bight. *Ocean Modell.* 33, 270–282. doi:10.1016/j.ocemod.2010.03.001.
- Shchepetkin, A.F., McWilliams, J.C., 2005. The regional oceanic modeling system (ROMS): a split-explicit, free-surface, topography-following-coordinate oceanic model. *Ocean Modell.* 9 (4), 347–404. doi:10.1016/j.ocemod.2004.08.002.
- Sommeria, J., 1986. Experimental study of the two-dimensional inverse energy cascade in a square box. *J. Fluid Mech.* 170, 139–168. doi:10.1017/S0022112086000836.
- Stanev, E., Schulz-Stellenfleth, J., Staneva, J., Grayek, S., Seemann, J., Petersen, W., 2011. Coastal observing and forecasting system for the German Bight. Estimates of hydrophysical states. *Ocean Sci.* 7, 1–15. doi:10.5194/os-7-569-2011.
- Stanev, E., Ziemer, F., Schulz-Stellenfleth, J., Seemann, J., Staneva, J., Gurgel, K.-W., 2015. Blending surface currents from HF radar observations and numerical modelling: tidal hindcasts and forecasts. *J. Atmos. Ocean. Technol.* 32, 256–281. doi:10.1175/JTECH-D-13-00164.1.
- Sündermann, J., Pohlmann, T., 2011. A brief analysis of North Sea physics. *Oceanologia* 53 (3), 663–689. doi:10.5697/oc.53-3.663.
- Veneziani, M., Edwards, C., Moore, A., 2009. A central California coastal ocean modeling study: 2. Adjoint sensitivities to local and remote forcing mechanisms. *J. Geophys. Res.: Oceans* (1978–2012) 114 (C4), 1–20. doi:10.1029/2008JC004775.
- Zhang, Y.J., Stanev, E., Grashorn, S., 2016. Unstructured-grid model for the North Sea and Baltic Sea: Validation against observations. *Ocean Modell.* 97, 91–108. doi:10.1016/j.ocemod.2015.11.009.